

**JSUM Ultrasound Elastography Practice Guidelines
Basics and Terminology**

Tsuyoshi Shiina

Department of Human Health Sciences, Graduate School of Medicine, Kyoto University, Kyoto, Japan

Abstract

Ten years have passed since the first commercial equipment for elastography was released, and the clinical utility has been demonstrated. Nowadays, most manufacturers offer an elastography option. The most widely available commercial elastography methods are strain imaging, using external tissue compression and generating images of the resulting tissue strain. However, the imaging method differs slightly between manufacturers, which results in differences in image characteristics like spatial and temporal resolution and differences in the recommended measurement conditions. In addition, recently many manufacturers have provided shear wave based method, which provide stiffness images based upon the shear wave propagation speed. Each method of elastography is designed based on assumption of measurement condition and tissue properties. Then we need know the basic principles of elastography methods and the physics of tissue elastic properties in order to use appropriately the each equipment and obtain more precise diagnostic information from elastography. From this standpoint, the basic section of this guideline is formed to support practice of ultrasound elastography.

Keywords:

Tissue elasticity, stiffness, elastography, strain, shear wave, acoustic radiation force

1. Introduction

It is known that changes in the stiffness of tissue are involved in various diseases such as cancerous masses, fibrosis associated with liver cirrhosis, and atheroma and calcification associated with arteriosclerosis. While a variety of techniques such as CT, MRI, and PET are being put to practical use for diagnostic imaging of morphology and function, it can be said that a technique for objectively detecting the stiffness of tissues was only recently made available with the practical application of elastography using ultrasound. Some examples of the clinical usefulness of measurement of the stiffness of tissues are as follows.

- 1) Use in early detection and differential diagnosis of diseases since it may reflect qualitative changes even in the case that morphological changes do not make an appearance.
- 2) Improvement in accuracy for diagnosing diseases with sclerotic lesions of tissue such as cancer, chronic hepatitis and arteriosclerosis by evaluating the extent of lesions and the degree of progression.
- 3) Assessment of response to treatments such as radiofrequency ablation and chemotherapy

In the case of uniform materials such as rubber, the stiffness can be easily expressed using the elastic modulus that will be described below, but in the case of biological tissue, there are a variety of factors that determine the stiffness. At the micro level, the factors are related to the composition of tissue such as fat and fiber components. For example, it is known that arteriosclerotic plaque becomes stiffer as the composition changes from lipid to calcification with disease progression. At the macro level, it is known that spiculated tissue formed around cancer is resistant to deformation, consequently it is felt as a hard area on palpation. Therefore, tissue elasticity will differ depending on what level is being observed. Moreover, the elasticity of biological tissue, which is anisotropic and nonlinear, will differ depending on the direction and extent of the deformation.

However, there is no question that an elastic modulus determined based on several assumptions will show a high correlation with disease. For example, as shown in Table 1 [1], the results of mechanical measurement of the resected breast cancer tissue showed that its elastic modulus (Young's modulus) was significantly higher than that of the normal gland tissue [1-3].

2. Principle of elastography

2.1 Measured physical quantity and excitation methods

Differences in the elasticity of the soft tissue are expressed by elastic modulus such as Young's modulus E , and shear modulus G , and we can deduce that elastic modulus can be calculated in the following two ways with respect to the directly- measured quantities (see the relational equations in Appendix) ,

- 1) Calculate E by using the following equation (Hooke's law, Eq. (A1) in Appendix) after externally applying stress σ and measuring strain ϵ ,

$$E = \sigma / \epsilon \quad (1)$$

- 2) Calculate E or G by using Eq. (2) (derived from Appendix Eqs. (A7) and (A9)) after propagating shear waves (transverse waves) and measuring the propagation speed c_s .

$$E \doteq 3G = 3\rho c_s^2 \quad (2)$$

Here, we assume that Poisson's ratio of soft tissue is near 0.5 of an incompressible medium, which is mostly correct (Eq. (A7)). Thus, Young's modulus will be equal to about three times that of the shear modulus.

Research on elastography started at the same time in the early 1990s for both of the above methods [4,5]. At that time, the former was called the (quasi-) static method and the latter the dynamic method according to how the external mechanical excitation was applied, but here we will refer to them as strain imaging and shear wave imaging respectively, according to the measured physical quantity.

Both of the above methods require external excitation. In other words, a dynamic action (compression or vibration) are externally applied to tissue to produce the reaction such as deformation or shear wave propagation, and physical quantity such as deformation (or strain) and propagation speed are measured by using ultrasound to estimate elasticity, as shown in Fig. 1.

2.2 Classification of elastography methods

Excitation methods can be divided into (A) Manual compression (using hand or cardiovascular pulsation), (B) Acoustic radiation force impulse, and (C) Mechanical impulse.

Therefore, elastography is classified as shown in Table 2a based on differences in the measured physical quantity and the excitation method. As far as methods to be integrated into clinical practice are concerned, they are categorized into four groups as follows,

Group 1: Strain elastography

Strain induced by quasi-static methods such as manual compression or cardiovascular pulsation is measured, and the distribution of strain or its normalized values within ROI is displayed.

Group 2: ARFI (acoustic radiation force impulse) imaging

A focused acoustic radiation force 'push' pulse is used to deform the tissue. The resulting tissue displacement is monitored. Although strain is spatial differential of displacement, they are similar since both are inversely related to the tissue stiffness.

Group 3: Shear wave based elastography

Acoustic radiation force is used to generate shear waves within the organ of interest. There are two modes of using shear wave speed. One is point shear wave elastography which is performed in a small region of interest compared to the field of view in the image. The other is shear wave elastography, which images distribution of speed or elastic modulus converted by equation (2).

Group 4: Transient elastography

Mechanical impulse or vibrating ‘punch’ is used to generate shear waves. At present, commercialized technology is specialized for measuring stiffness of liver tissues and not for imaging.

Outputs obtained by each elastography technology correspond to a measured physical quantity, that is, measures based on strain or shear wave speed as shown in Table 2b. As for strain, geometric measures such as size or shape of the low strain area, the strain ratio of the lesion to reference and E/B size ratio (ratio of the size of a lesion in the strain image to its size in the B-mode image). As for shear wave based methods, the physical quantity is speed itself and/or Young’s modulus converted from shear wave speed on assumptions of constant density, homogeneity, isotropy, and incompressibility using Eq. (2). The characteristics of each technology are described below.

3. Strain imaging

3.1 Strain elastography

The first style of elastography put to practical use is a method for measuring the tissue deformation generated by manually applying pressure with a probe on the body surface, similar to palpation, or by cardiovascular pulsation. It is classified as strain elastography in Table 2. This method has been commercialized by manufacturers and is currently being used in various fields of clinical medicine including breast diagnosis.

This method was first referred to as elastography by Dr. Ophir from the University of Texas [4,6]. As shown in Fig. 2, when very slight pressure (about 1%) is applied to tissue with a probe in the beam direction, the majority of the displacement will be in the direction of the propagation of the ultrasound pulse, and the tissue deformation can be approximated using a 1D spring model. Displacement $\delta(z)$ at each site z in the beam direction of the tissue is then calculated. This is obtained by calculating the correlation between the echo signal before and after compression. Next, strain ε is obtained by spatial differential of displacement, that is, a ratio of the difference in displacement between two points to their distance of pre-compression, L , as shown in Eq. (3):

$$\varepsilon = \frac{d\delta}{dz} \rightarrow \frac{\delta_2 - \delta_1}{L} \quad (3)$$

In actuality, as described herein below, many technologies must be developed to achieve real-time capability, accuracy, and stability during manual compression before it becomes available for clinical application [7-11].

As shown in Equation (1), Young's modulus E can be obtained if stress σ and strain ε are known. However, since it is difficult to actually calculate the stress distribution *in vivo*, it is assumed to be uniform. As a result, stiff segments with a large elastic modulus E will have a small strain ε ; therefore, strain serves as a useful indicator from the standpoint of evaluating relative stiffness.

With respect to manual compression from the body surface, it is possible to apply pressure up to the normal diagnostic depth in the case of organs near the surface of the body such as the mammary gland and thyroid gland, but stress is not easily transmitted to deep organs such as the liver, making it difficult to elicit strain. Therefore, strain induced by either cardiovascular pulsation or respiration is used for the evaluation of liver fibrosis with strain imaging [12].

3.2 Practical system of strain elastography

The first practical application of ultrasound elastography in 2003 was strain imaging employing manual compression with a probe, similar to an ordinary ultrasound examination (Fig. 3). Its efficacy was demonstrated in the diagnosis of breast cancer tumors together with elasticity score, which was proposed at the same time [13,14], and nowadays each manufacturer produces ultrasonographic equipment with a strain imaging function.

Strain imaging has the advantages of being easy to use and providing elasticity images with a high spatial resolution in a manner similar to palpation, i.e., tissue deformation. On the other hand, strain is a relative indicator of stiffness that changes depending on the degree of compression. Then, for example, the elastogram shown in Fig. 3(b) displays the normalized strain as the mean within the ROI in order to obtain stable images without being subjected to fluctuations in the intensity of compression.

Display methods of strain image

For clinical use, the display method of elastogram is an important factor since it is useful for diagnosis to easily relate the location in elastogram (strain image) to B-mode as a morphological image. Different types of display method are used for ultrasonographic equipment as shown in Fig. 4. For example, the method proposed by Dr. Ueno [14] and applied to the first practical equipment is as follows. The region of interest (ROI) to display tissue elasticity is specified on a B-mode image with the cursor, and the translucent elastogram within the ROI is superimposed on the corresponding B-mode image, with a color image; the average strain in the ROI is indicated in green, areas of low strain as stiff tissue are in blue, and areas of high strain as soft tissue are in red as shown in Fig. 4(a). Another type of display method is to display the elastogram with gray scale and B-mode image side-by-side as shown in Fig. 4(b). In this case, the location in the elastogram can be indicated on B-mode by the cursor.

Trial of quantitative evaluation based on strain imaging

As above mentioned, strain imaging is basically qualitative, so it is difficult to perform quantitative comparisons between cases using strain.

So far, imaging methods involving calculation of a more quantitative elastic modulus based on strain distribution are being investigated [15, 16], but the stress distribution must be estimated to achieve this. Therefore, easier and more pseudoquantitative methods are appearing. For example, there is a method in which a reference region where the change in elasticity caused by disease is minimal, such as fat in the mammary gland, is established, and the fat lesion ratio (FLR), which is the strain ratio between the fat and the lesion, is used as shown in Fig. 5(a) [17, 18]. The stiff, i.e., low-strain area reflects the size of tumor and is related with malignancy, and, it has been reported that malignant tumors often appear larger in strain images than in B-mode images, which has been attributed to desmoplasia. Consequently, as a quantitative diagnosis based on strain imaging, the size of the tumor in an elastogram is often measured and compared with the size of the low-echo area in B-mode as shown in Fig. 5 (b). Another example is a method for estimating the elastic modulus of a lesion based on the strain ratio using a coupler with a known elastic modulus [19]. In addition, as for the elastogram of diffuse disease such as chronic hepatitis, morphologic and statistic features are extracted and analyzed for the evaluation of the fibrous stage, which is described in the clinical session of this report.

Elasticity score

Strain images depict the relative difference in elasticity between lesions such as a mass and the surrounding tissue. Therefore, it is suitable for detecting patterns in images. In fact, the elasticity score (Tsukuba score) is being used for breast cancer diagnosis [14]. The elasticity score is a five-point scale used to classify elastography patterns from benign to malignant as follows: score 1 (benign), score 2 (benignancy suspected), score 3 (difficult to distinguish between benign/malignant), score 4 (malignancy suspected), and score 5 (malignancy strongly suggested) as shown in Fig. 6. In the case of cysts, a specific blue-green-red pattern called the BGR sign is seen from the body surface side. This is a type of artifact, but since the level of the internal echo signals from a cyst is low, this can be used for cyst diagnosis, like a lateral shadow on B-mode images.

3.3 Acoustic radiation force impulse (ARFI) Imaging

While strain elastography relies on manual application of pressure, a strain imaging method that deforms tissue using focused acoustic radiation force was devised. This method, called acoustic radiation force impulse (ARFI) imaging [20,21] has become commercially available within the past few years.

In this method, focused acoustic radiation force ‘push’ pulse is generated by Eq. (4) [22,23]

$$F = \frac{2\alpha I}{c} \quad (4)$$

(α : absorption coefficient, I : temporal average intensity of ultrasound, c : speed of sound)

Imaging pulses before and after application of a ‘push’ pulse, are used to monitor the tissue deformation (displacement) within the region of the ‘push’. The same transducer is used to both generate the push pulse and to monitor the resulting tissue displacement. The tissue displacement response is directly related to the magnitude of the applied force, and inversely related to the tissue stiffness. By sequentially interrogating different tissue regions with focused radiation force, and then synthesizing an image from the tissue response at a given time after the push (typically < 1msec), as shown schematically in Fig. 7, images of tissue displacement are generated that portray relative differences in tissue stiffness (Fig. 8), similar to the images generated in strain imaging. These images do not provide quantitative information about tissue stiffness because the magnitude of the applied radiation force varies with tissue attenuation from patient to patient and is difficult to quantify. This imaging approach is implemented commercially as Siemens Virtual Touch™ feature [24-27].

3.4 Appropriate measurement conditions and artifact for strain imaging

Many manufacturers provide elastography equipment employing strain imaging, but the imaging method differs slightly between manufacturers, and the recommended measurement conditions also differ. In terms of artifact in the strain imaging, it should be commonly noted that stress distribution is not uniform within the body, and tissue elasticity is nonlinear.

As above mentioned, based on Eq. (1), strain is used as the index of stiffness instead of Young’s modulus on the assumption that stress is uniform. However, in practice, stress tends to concentrate on curved boundaries so that strain increases along a boundary compared with adjacent area. This phenomenon causes the artifact that the part looks softer than the adjacent area as shown in Fig. 9. In many cases, this kind of artifact is easily recognized by a priori information such as a shape of tumor.

Regarding nonlinearity of tissue, in the case of biological tissue, Young's modulus tends to increase when the compression is intensified, as shown in Fig. 10, and the extent of the increase differs from tissue to tissue [28]. When the degree of compression is slight, therefore, the difference in Young's modulus between mammary gland tissue and tumor tissue, for example, is large, and the tumor tissue is appropriately displayed as a relatively low strain region, as shown in Fig. 11(a), but when the compression is too strong, the stiffness of the mammary gland will increase, and the difference from the tumor tissue will be smaller, possibly resulting in a false negative finding, as in Fig. 11(b).

The nonlinearity becomes marked when the compression generates strain in excess of several percent. However, when strain of about 1% (i.e., 0.3mm for a 3cm breast) is generated in the mammary gland, stability and reproducibility can be achieved even if the level of compression fluctuates since it is within the linear range. In the case of breast cancer diagnosis, one indicator is that pectoralis major muscle is uniformly blue or black in grayscale (small strain) when elastography is performed with proper compression, but when pectoralis major muscle is red (large strain) and the subcutaneous fat layer has blue mixed in, it often means that excessive compression has been used.

The ARFI imaging approach does not rely on the transducer compression technique as the strain elastography based on manual compression does, and it has the advantage of being able to focus the 'push' within deep lying organs without requiring fixed boundary conditions, where it can be difficult to generate deformation with compression from the body surface. On the other hand, this method can be depth limited, with most commercial implementations reaching the maximum depth of only about 75% of the corresponding B-mode images from a given transducer.

In addition, in order to generate detectable levels of strain, the 'push' pulses are of longer duration than regular diagnostic pulses. Therefore, in order to maintain acoustic output within diagnostic limits, current equipment enforces a certain amount of 'cooling' time after each measurement, which reduces the achievable frame rate of this imaging technique. Moreover, it is recommended that it should not be used in combination with an environment in which a physiological response to sound could easily occur in the body such as with use of contrast agents [29-30].

The method that employs acoustic radiation force requires appropriate focusing of pulse waves for applying pressure in order to generate tissue displacement. As such, it can be affected by the inhomogeneous properties of tissue. In addition, tissue stiffens when the compression applied by the probe is intensified, because of the nonlinearity of tissue elasticity. Therefore, the method employing acoustic radiation force also requires technique to maintain the optimal conditions.

4. Shear wave imaging

Shear wave imaging is based on the theory that the speed of shear wave propagation, c_s , through tissues is related to the stiffness of tissues. The relation is expressed by Eq. (2), that is, elastic modulus, E , is proportional to the square of the speed of shear wave propagation, $E=3\rho c_s^2$, on the assumption of simple material, that is, linear, isotropic, incompressible and homogeneous.

Shear waves can be generated from a variety of sources, including external vibration, physiological motion, and acoustic radiation force. Table 2 shows the commercially available shear wave imaging systems. There are two methods of mechanical excitation and acoustic radiation force based methods as shown in Fig. 12. Mechanical excitation is applied to Transient Elastography where an external vibrating ‘pinch’ is used to generate shear waves as shown in Fig. 12(a). At present, commercialized technology is specialized for measuring stiffness of liver tissues and not for imaging.

As for acoustic radiation force, focused ultrasound beams are used to generate shear waves within the ROI as shown in Fig. 12 (b). There are two modes of using shear wave speed. One is point shear wave elastography, which is performed in a small region of interest compared to the field of view in the image. The other is shear wave elastography, which images distribution of speed or elastic modulus converted on assumptions of constant density, homogeneity, isotropy, and incompressibility using Eq. (2).

4.1 Transient elastography

In this method, which is currently used in FibroScanTM for evaluation of liver fibrosis, short pulsed vibrations (about 50 Hz) like those shown in Fig. 13(a) are applied to the body surface using a vibration exciter. As a result, shear waves generated near the body surface propagate within the liver. By using a way similar to the Doppler method to calculate the distribution of tissue displacement that occurs as a result of propagation of these shear waves, an image showing the relationship between distance and propagation time, like that shown in Fig. 13(b), can be obtained. The shear wave propagation speed c_s [m/s] is obtained based on the slope corresponding to the peak point of this displacement. Using ρ [kg/m³] as the density, elasticity (Young's modulus) E [kPa] is calculated as $E=3\rho c_s^2$.

4.2 Shear wave elastography

In response to a focused acoustic radiation force excitation, in addition to vibrating at the ultrasonic frequency, the tissue within the region of excitation (ROE) is also deformed, and shear waves are created that propagate away from the ROE in a direction orthogonal to the excitation beam as shown in Fig. 14(a). Figure 14 (b) shows the displacement through time profiles at the focal depth of radiation force excitation at three different lateral positions. By comparing this waveform between adjacent positions, propagation time T is obtained. Shear wave speed estimates are generated by calculating the ratio of distance, d , to propagation time, T . In actuality, the speed is obtained based on the slope of the approximation line on a graph of the distance and propagation time for a measurement point obtained using multiple detection beams within a sample volume, as shown in Fig. 14(c), in order to improve the accuracy.

Since acoustic radiation force is applied at a single focal location, imaging requires generation of shear waves at multiple points throughout imaging area, which reduces the frame rate. Another approach is a multi-focal zone configuration in which each focal zone is interrogated in rapid succession, leading to a cylindrically shaped shear wave extending over a larger depth, enabling real-time shear wave images to be formed as shown in Fig. 15. This approach has been termed supersonic shear imaging, as implemented by ShearWaveTM elastography (SWE) [31].

Whichever generation method is used, shear wave imaging can be used to estimate E using Eq. (2) by calculating the distribution of c_s . Making use of its quantitative capability, it is used not only for imaging

but also for numerically calculating tissue elasticity. Although it is a merit of shear wave imaging that the elastic modulus is obtained without estimating stress, it is to be noted that Eq. (2) folds on the assumption of simple material, that is, linear, isotropic, incompressible and homogeneous.

At the same time, the apparent elasticity associated with propagation speed will change with internal pressure caused by blood pressure, etc., so it may be different from elasticity caused by fibrosis. In fact, it has been reported that the speed increases during inflammation due to jaundice [32]. In addition, apparent elastic modulus G' in Eq. (A10) will be larger than elastic modulus G obtained by static compression when the viscosity is high. Figure 16 shows the difference in the frequency dependence of speed due to presence of viscosity.

4.3 Appropriate measurement conditions and artifact for shear wave imaging

In shear wave imaging, Young's modulus is estimated by generating shear waves in the body and measuring their propagation speed. Therefore, measurement conditions to be considered for appropriate imaging and possible artifact in a clinical setting are as follows.

a) Intensity of excitation acoustic force and heterogeneity of distribution

A method of generating shear waves by tissue compression using acoustic radiation force requires that pulse waves for excitation appropriately form a focal point in the body. Therefore, when contact between the probe and the surface of the body is inadequate, or when the angle of incidence is inappropriate, sufficient acoustic force for excitation cannot be achieved at the affected area, resulting in shear waves not being appropriately generated. This causes artifacts and failed measurements.

b) Effects of refraction/reflection of shear waves

As described in appendix (A.1), the range of the shear wave speed in tissue is large, i.e., 1-10 m/s, unlike longitudinal waves used in B-mode US, which are about the same as the acoustic velocity in water, i.e., about 1500 m/s. This means that shear waves are greatly refracted at the tissue interface where the acoustic speed differs. Likewise, the difference in the characteristic acoustic impedance of tissue to shear waves is also large, sometimes resulting in the reflection coefficient at the soft tissue margin being large as compared with longitudinal waves.

In the case of malignant tumors, in particular, the acoustic velocity changes at the tumor site because it stiffens relative to the surrounding tissue, and the inside of the mass often has a heterogeneous structure and property; therefore, the likelihood of marked wave phenomena caused by refraction and reflection occurring is high. The change in the propagation direction caused by refraction must be determined in order to accurately calculate the acoustic velocity of shear waves to obtain Young's modulus using shear wave imaging. In addition, incident waves and reflected waves are observed as compound waves at the tissue margin, but the incident waves alone must be measured by separating them by acoustic speed. For actual diagnostic equipment, adjustments must be made to produce reliable images and measurements in a more convenient manner, such as assuming the propagation direction, in order to emphasize their real-time capability, which is the advantage of ultrasonography.

At the present time, they need to be use

d for diagnosis with the understanding that artifacts and variations in measurements will occur. Owing to its quantitiveness, shear wave imaging yields elastic characteristics as numerical values, not patterns, but the results need to be interpreted carefully, keeping in mind the conditions under which the results were obtained and determining whether the measurements contain artifacts.

4.4 Relationship between strain and shear wave speed images

Both strain and shear wave speed images provide information related to the underlying tissue stiffness. As such, in the absence of artifacts, the correlation between these image types in a given patient is expected to be high. In general, strain images exhibit higher spatial resolution, and shear wave images will have higher contrast [33]. However, when the simplifying assumptions used to derive the images for the different methods do not accurately reflect the tissue behaviors, differences between the images from the different techniques can be anticipated. Tissue nonlinearity is associated with decreased strain contrast (Fig. 16) and increased shear wave speeds when excessive transducer compression is applied. As a result, for both strain and shear wave imaging, minimizing the amount of transducer compression used during imaging (i.e less than 1%) will result in the most reproducible imaging scenario. Tissue heterogeneities will also impact both approaches, leading to artifacts arising from reflected waves in shear wave speed images, and strain concentrations surrounding tissue heterogeneities. A more detailed investigation of the impact of these assumptions and associated image artifacts should be carried out in the future.

5. Conclusion

Tissue elasticity imaging further improves the value of ultrasonography by combining the characteristic features of ultrasound, i.e., noninvasiveness, real-time capability, and ease of use, with the ability to provide new diagnostic information related to tissue characterization. The first practical equipment for elastography was released in 2003, but today every manufacturer offers a compressive elastography unit, and many manufacturers offer both strain and shear wave based approaches. This fact could be considered a testament to the utility of elasticity imaging. On the other hand, it is still an evolving technology with much technical potential for clinical application in the future including expanding its scope of application, quantification, 3D measurement, and treatment support, etc. One might anticipate that it will further evolve in the future and attain a position equal to that of Doppler as a new mode of ultrasound imaging.

Appendix

A.1 Tissue Biomechanics [34-37]

Stiffness is resistance to deformation, and application of external force is required to measure it. The behavior exhibited when force is applied to tissue is described as a viscoelastic body with viscosity and elasticity, and it can be approximated using the model shown in Fig. A1. As shown in Fig. A1(a), the stress σ (equal to external force per unit area) and strain ε (equal to expansion per unit length) exhibit proportionality, as known in Hooke's law in Equation (A1), and its coefficient is elastic modulus Γ .

$$\sigma_1 = \Gamma \cdot \varepsilon \quad (\text{A1})$$

As shown in Fig. A1(b), as for the viscosity component, stress σ_2 is proportional to the speed of deformation, i.e., strain rate $d\varepsilon/dt$, and its coefficient μ is the viscosity coefficient.

$$\sigma_2 = \mu \frac{d\varepsilon}{dt} \quad (\text{A2})$$

The mechanical characteristics of general tissue consist of a complex combination of elastic and viscous components, which are often approximated using a simplified model like that in (c). Where the speed of the applied external force is slow such as manual compression, and the effect of viscosity can be disregarded in Eq. (A2), the model shown in (c) can approximate the dynamic properties with only the elastic component (a). Conversely, if high-frequency vibration is applied, the viscous component will have a major effect, the extent of which will depend on the frequency.

With regard to elasticity, three types of elastic moduli (Young's modulus, shear modulus, and bulk modulus) are defined based on the method of deformation. Young's modulus E is defined by the following equation when stress is applied longitudinally to a long, thin cylindrical object, and strain occurs as shown in Fig. A2(a).

$$\sigma = E \cdot \varepsilon_L \quad (\text{A3})$$

where σ is stress and $\varepsilon_L = \Delta L/L$ is (longitudinal) strain.

In the absence of volume change, a cylindrical object becomes thinner when stretched in Fig. A2. The percent change in the radial direction, $\varepsilon_r = \Delta r/r$, is called transverse strain, and the ratio of longitudinal strain to transverse strain,

$$\nu = \frac{\varepsilon_r}{\varepsilon_L} \quad (\text{A4})$$

is called Poisson's ratio. Poisson's ratio indicates the extent of volume change caused by deformation, and ν will be no higher than 0.5 in the case of an incompressible medium.

Shear modulus G is defined by the following equation for the shear deformation shown in Fig. A2(b).

$$\sigma = G \cdot \varepsilon_s \quad (\text{A5})$$

where $\varepsilon_s = \theta$ is shear strain.

Bulk modulus K is defined by the following equation when the volume changes under pressure.

$$\sigma = K \cdot \varepsilon_v \quad (A6)$$

where $\varepsilon_v = \Delta V/V$ is volume strain. The larger the elastic modulus is, the smaller the strain will be with the same stress, so it will be stiffer. For example, Young's modulus E is expressed as in Eq. (A7) using shear modulus G and Poisson's ratio ν . The water content of soft tissue is high, and consequently its Poisson's ratio is near 0.5 of an incompressible medium, so Young's modulus will be equal to about three times of the shear modulus, as in the following equation.

$$\begin{aligned} E &= 2(\nu + 1)G \\ &\doteq 3G \end{aligned} \quad (A7)$$

Thus, the elastic modulus is defined for static deformations, but it is also a component that determines the propagation velocity of waves. Wave propagation generally involves **longitudinal waves** and **transverse waves**, as shown in Table A1. In other words, in the case of ordinary ultrasound images used or pulse-echo imaging, longitudinal waves are used, and the speed c_L of the longitudinal waves is

$$c_L = \sqrt{\frac{K}{\rho}} \quad (A8)$$

where ρ indicates the density of the medium. Using the shear modulus, the speed c_s of transverse waves is expressed as

$$c_s = \sqrt{\frac{G}{\rho}} \quad (A9)$$

Equations (A8) and (A9) indicate that the larger K and G are, i.e., the stiffer the medium is, the faster the wave will propagate. In the case of soft tissue, it is known that the speed of a longitudinal wave is about the same as the sound speed in water ($c_L=1500$ m/s), but this means that there is little difference in K between tissues. In contrast, transverse waves, which are also called shear waves, attenuate rapidly and disappear in the MHz ultrasound band, but attenuation decreases and they can propagate *in vivo* when the frequency is below about 1 kHz. Moreover, their velocity is quite slow, i.e., $c_s=1-10$ m/s, as compared with longitudinal waves, so G is low, i.e., 1-100 kPa, and the difference between tissues is large, which enables us to reconstruct images with high tissue contrast [35].

On the other hand, unlike the static deformation, velocity dispersion caused by viscosity occurs during wave propagation when the frequency is high in soft tissues. For example, when the Kelvin-Voigt model is used (Fig. A1(c)), the following equation is used for the speed of a transverse wave instead of Eq. (A9) as a result of taking into account viscosity [38].

$$c_s = \sqrt{\frac{2\{G^2 + (2\pi\mu f)^2\}}{\rho\{G + \sqrt{G^2 + (2\pi\mu f)^2}\}}} \quad (A10)$$

Thus, it becomes the function of frequency f , and the higher the frequency is, the faster the speed will be.

A.2 Displacement measurement

In strain imaging, displacement in the direction of pulse propagation is measured to calculate strain, while in shear wave speed imaging, the displacement of tissue in the direction perpendicular to the shear wave propagation is measured to calculate speed of shear wave propagation. Therefore, measurement of displacement is a key technology in all elastography techniques, and there are several methods for measuring it. As shown in Table 2, strain imaging, is now installed in ultrasound equipment of many manufacturers, but each manufacturer uses its own method for measuring displacement, which results in differences in image characteristics like spatial and temporal resolution and differences in optimal measurement conditions.

The typical methods for measuring displacement are shown below.

(1) Spatial correlation method (speckle tracking method, pattern matching method)

This is a method that tracks the movement of image patterns. Since patterns move while maintaining the speckle pattern in the case of extremely slight strain, in this method the amount of movement, i.e., displacement, is sought by setting a region of interest (ROI) and calculating the spatial correlation of the ROI before and after compression. The simplest method is to measure 1D displacement along the beam axis as shown in Fig. A3(a), using a time window $w(z;t)$ centered around the measurement point at depth z , and with the waveform with echo signals $s(t)$ and $s'(t)$ before and after compression clipped out expressed as Eq. (A11), the cross-correlation coefficient in Eq. (A12) is calculated to evaluate the degree of similarity. Calculation of the cross-correlation coefficient is repeated while moving the window, and displacement is defined as the amount of movement when the value is at its maximum.

Model of echo signals clipped out in time window $w(z;t)$

$$\begin{aligned} \text{Before compression: } x(z;t) &= w(z;t) [s(t)] \\ \text{After compression: } y(z;t) &= w(z;t) [s'(t)] \end{aligned} \quad (\text{A11})$$

Cross-correlation coefficient:

$$R(\delta) = \frac{\int x(z;t)y(z+\delta;t)dt}{\sqrt{\int x^2(z;t)dt \int y^2(z+\delta;t)dt}} \quad (\text{A12})$$

In reality, each ROI moves in the azimuth direction in the cross section, so the maximum correlation does not necessarily fall within the destination of the ROI simply by moving the correlation window in the range direction. Therefore, an adjustment is made to more accurately obtain displacement by performing a 2D search in both the range direction and the azimuth direction, as shown in Fig. A3(b). In addition, tissue also moves in the slice direction, but the beam width in the slice direction is generally large in the case of an ordinary electronic scanning probe, so the impact is smaller than the azimuth direction as long as the cross section does not deviate much.

(2) Phase difference detection method (Doppler method)

As shown in Fig. A4, this is basically the same method as that used in color Doppler and tissue

Doppler [39]. In this method, the phase difference between echo signals obtained by transmitting repeated pulses is detected by the autocorrelation method to calculate the displacement.

As shown in Table A2, the advantages of the Doppler method are its excellent real-time capability and its relative robustness against noise, but only 1D displacement in the beam direction can be measured due to angle dependence, and errors occur due to aliasing when measuring large displacement that exceeds half the wavelength.

The advantages of the speckle tracking method are that it is possible to measure even large displacement that exceeds the wavelength if the change in the speckle pattern is within a small range, and it is possible to track the movement of the ROI in 2D and 3D, as stated above. However, the disadvantage is that the real-time capability may be lost because calculation of correlation requires enormous computation. In addition, it is susceptible to the effects of noise, and it is prone to detection errors when the speckle pattern is unclear due to a low echo level, etc.

(3) Combined method

From the standpoint of practical application in a clinical setting, a high degree of accuracy to accommodate small displacement and a dynamic range wide enough to handle large displacement are necessary since fluctuations in the speed of compression are large in the case of manual compression. In addition, deformation occurs not only in one dimension in the beam direction but also in the azimuth direction, due to lateral slippage of the probe and unsteady hands, etc. Moreover, the real-time capability is critical along with accuracy. Thus, a combined autocorrelation method that combines the merits of the phase difference detection method and the spatial correlation method was developed [9,13]. As shown in Fig. A5, the rough displacement is first calculated from the envelope using the resolution of half a wavelength, and then the displacement is calculated in high resolution using the phase difference after correcting the rough displacement. As a result, it has a wide dynamic range and provides high accuracy, being able to accommodate strain ranging from about 0.05% to 5% without causing aliasing errors, for not only displacement less than a wavelength but also large displacement. Since both processes use the autocorrelation method used in color Doppler, it achieves high speed, high accuracy, and a wide dynamic range for detecting displacement, as a result, the method is suitable to actual manual compression. Therefore, it was installed in the first equipment that was put to practical use, and it is currently being used in a 3D elastography system.

In the case of actual equipment, improvements have been made for the above-mentioned spatial correlation method and phase difference detection method, and they are being used in the practical equipment, but differences in their characteristics manifest as differences in frame rate, image quality, and measurement conditions, etc.

References

- [1] Samani A, Zubovits J, Plewes D. Elastic moduli of normal and pathological human breast tissues: an inversion-technique-based investigation of 169 samples. *Phys Med Biol* 2007;52(6):1565-76.
- [2] Krouskop TA, Wheeler TM, Kallel F, et al. The elastic moduli of breast and prostate tissues under compression. *Ultrason Imaging* 1998;20(4):260-74.
- [3] Wellman PS, Howe RD, Dalton E, et al. Breast tissue stiffness in compression is correlated to histological diagnosis. Harvard BioRobotics Laboratory, Technical Report, 1999.
- [4] Ophir J, Cespedes I, Ponnekanti H, et al. Elastography: a quantitative method for imaging the elasticity of biological tissues. *Ultrason Imaging* 1991; 13:111–34.
- [5] Parker KJ, Huang SR, Musulin RA. Tissue response to mechanical vibrations for sonoelasticity imaging. *Ultrasound Med Biol* 1990;16:241–6.
- [6] Parker KJ, Doyley MM, Rubens DJ. Imaging the elastic properties of tissue: the 20 year Perspective. *Physics in Medicine and Biology* 2011;56:R1-R29.
- [7] Bamber JC, Bush NL. Freehand elasticity imaging using speckle decorrelation rate. *Acoust Imaging* 1996;22:285–92.
- [8] Bamber JC, Barbone PE, Bush NL, et al. Progress in freehand elastography of the breast. *IEICE Trans Inf. Syst* 2002; E85D, 5–14.
- [9] Shiina T, Doyley MM, Bamber JC. Strain imaging using combined RF and envelope autocorrelation processing. *Proc. of 1996 IEEE Int. Ultrasonics Symposium*, 1331-6, 1996.
- [10] Varghese T, Ophir J. A theoretical framework for performance characterization of elastography: the strainfilter. *IEEE Trans. Ultrason. Ferroelectr. Freq. Control* 44:164–172, 1997.
- [11] Hall TJ, Zhu YN, Spalding CS. In vivo real-time freehand palpation imaging. *Ultrasound Med Biol* 2003;29:427–35.
- [12] Morikawa H, Fukuda K, Kobayashi S, et al. Real-time tissue elastography as a tool for the noninvasive assessment of liver stiffness in patients with chronic hepatitis C. *J Gastroenterol* 2011;46:350-8.
- [13] Shiina T, Nitta N, Ueno E, et al. Real time elasticity imaging using the combined autocorrelation method. *J Med Ultrasonics* 2002;29:119–28.
- [14] Itoh A, Ueno E, Tohno E, et al. Breast disease: clinical application of US elastography for diagnosis. *Radiology* 2006;239(2):341-50.
- [15] Barbone PE, Gokhale NH. Elastic modulus imaging: on the uniqueness and nonuniqueness of the elastography inverse problem in two dimensions *Inverse Probl.* 2004; 20: 283–96.
- [16] Fehrenbach J. Influence of Poisson's ratio on elastographic direct and inverse problems *Phys. Med Biol* 2007;52:707–16.
- [17] Ueno E, Tohno E, Bando H, et al. New quantitative method in breast elastography: Fat Lesion ration (FLR). *Abstract of RSNA 2007*; LL-BR2123-H04.
- [18] Farrokh A, Wojcinski S, Degenhardt F, et al. Diagnostic value of strain ratio measurement in the differentiation of malignant and benign breast lesion. *Ultrasound Med* 2011;32(4):400-5.
- [19] Matsumura T. Measurement of elastic property of breast tissue for elasticity imaging. *Proc. of 2009 IEEE Ultrasonics Symposium*. 1451-4, 2009.
- [20] Nightingale K, Bentley R, Gregg ET. Observations of tissue response to acoustic radiation force: opportunities for imaging. *Ultrasonic Imaging* 2002; 24(3):129–38.
- [21] Nightingale K, Soo MS, Nightingale R, et al. Acoustic radiation force impulse imaging: in vivo demonstration of Clinical Feasibility. *Ultrasound Med Biol* 2002;28(2):227–35.
- [22] Nyborg WLM, Litovitz T, Davis C. Acoustic streaming. In: Mason WP (eds). *physical acoustics*. New York, Academic Press Inc; 1965. P. IIA 265–331.

- [23] Torr GR. The acoustic radiation force. *Am J Phys* 1984;52:402–8.
- [24] Seung Hyun Cho, Jae Young Lee, Joon Koo Han, et al. Acoustic Radiation Force Impulse Elastography for the Evaluation of Focal Solid Hepatic Lesions: Preliminary Findings. *Ultrasound in Medicine & Biology* 2010;36(2):202–8.
- [25] D'Onofrio M, Gallotti A, Salvia R, et al. Acoustic radiation force impulse (ARFI) ultrasound imaging of pancreatic cystic lesions. *European Journal of Radiology* 2011;80(2):241–4.
- [26] Gallotti A, D'Onofrio M, Mucelli RP. Acoustic radiation force impulse (ARFI) technique in the ultrasound study with virtual touch tissue quantification of the superior abdomen. *Radiol Med* 2010;115(6):889–97.
- [27] Clevert DA, Stock K, Klein B. Evaluation of acoustic radiation force impulse (ARFI) imaging and contrast-enhanced ultrasound in renal tumors of unknown etiology in comparison to histological findings. *Clinical Hemorheology and Microcirculation* 2009;43(1-2):95–107.
- [28] Barr RG, Zhang Z. Effects of precompression on elasticity imaging of the breast-development of a clinically useful semiquantitative method of precompression assessment. *J Ultrasound Med* 2012;31:895–902.
- [29] Barnett SB, Duck F, Ziskin M. Recommendations on the safe use of ultrasound contrast agents. *Ultrasound in Medicine & Biology* 2007;33:173–4.
- [30] Ultrasound Equipment and Safety Committee of The Japan Society of Ultrasonics in Medicine. Safe use of imaging equipment using acoustical radiation force.
(http://www.jsum.or.jp/committee/m_and_s/acoustic_radiation.html)
- [31] Deffieux T, Montaldo G, Tanter M, et al. Shear wave spectroscopy for in vivo quantification of human soft tissues visco-elasticity. *IEEE Trans. on Medical Imaging* 2009;28(3):313–22.
- [32] Fujimoto K, Kato M, Kudo M, et al. Novel image analysis method using ultrasound elastography for noninvasive evaluation of hepatic fibrosis in patients with chronic hepatitis C. *Oncology* 2013;84(suppl1):3–12.
- [33] Palmeri ML, Michael HW, Ned CR, et al. Noninvasive evaluation of hepatic fibrosis using acoustic radiation force-based shear stiffness in patients with nonalcoholic fatty liver disease. *Journal of Hepatology* 2011;55(3):666–72.
- [34] Duck FA. *Physical properties of tissues*. New York, Academic press, 1990.
- [35] Sarvazyan A, Hill CR. Physical chemistry of the ultrasound-tissue interaction. In: Hill CR, Bamber JC, ter Haar GR (eds). *Physical Principles of Medical Ultrasonics*, 2nd Edition. Chichester, John Wiley; 2004. p. 223–35.
- [36] Parker KJ, Taylor LS, Gracewski S, et al. A unified view of imaging the elastic properties of tissue. *J Acoust Soc Am* 2005;117(5):2705–12.
- [37] Greenleaf JF, Fatemi M, Insana M. Selected methods for imaging elastic properties of biological tissues. *Annu Rev Biomed Eng* 2003;5:57–78.
- [38] Deffieux T, Montaldo G, Tanter M, et al. Shear wave spectroscopy for in vivo quantification of human soft tissues visco-elasticity. *IEEE Trans. on Medical Imaging* 2009;28(3):313–22.
- [39] Thomas A, Warm M, Hoopmann M, et al. Tissue Doppler and strain imaging for evaluating tissue elasticity of breast lesions. *Acad Radiol* 2007;14(5):522–9.

Figure legend

Figure 1

Concept of measurement of tissue elasticity

Figure 2

Principle of strain elastography

Figure 3

Practical application of strain imaging

Figure 4

Different display methods of strain image (by courtesy of SIEMENS)

Figure 5

Quantitative diagnosis based on strain imaging

Figure 6

Elasticity score in breast cancer diagnosis

Figure 7

Pulse sequence in ARFI imaging. ARFI imaging utilizes acoustic push pulses and tracking beams, sequenced across a user-defined region of interest, to generate an elastogram depicting the relative stiffness of tissue.

Figure 8

An image by ARFI imaging

Figure 9

Artifacts due to stress concentration

Figure 10

Change in contrast according to nonlinearity of tissue elasticity. When compression is increased, the tissue stiffens and the contrast between fat and a cancerous mass decrease.

Figure 11

Effect of excessive compression (breast cancer)

Figure 12

Shear wave generation methods

Figure 13

Principle of transient elastography (FibroScan™)

Figure 14

Measurement of propagation speed of shear waves

Figure 15

Shear wave excitation and high-speed measurement by SWE. Shear waves are generated by multi-focal zone configuration in which each focal zone is interrogated in rapid succession, leading to a cylindrically shaped shear wave extending over a larger depth as shown in (a). Unlike the regular method of focusing during transmission, by simultaneously performing aperture synthesis by transmitting plane waves for the displacement detection method as shown in (b), the incoming data are acquired at high speed, i.e., about 5,000 frames/sec, which is almost 100 fold, and the propagation velocity distribution within the ROI is obtained.

Figure 16

Difference in propagation velocity according to presence or absence of viscosity ($G = \text{kPa}$, $\mu = \text{Pa} \cdot \text{s}$)

Figure A1
Viscoelastic model

Figure A2
Various elastic moduli

Figure A3
Calculation of correlation using spatial correlation method

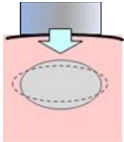
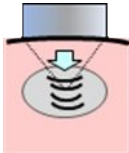
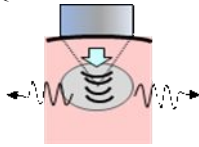
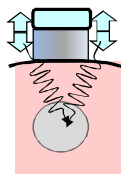
Figure A4
Measurement of displacement by phase difference detection method

Figure A5
Principle of the combined autocorrelation method

Table 1 Young's modulus of breast tissue samples [1]

Breast tissue type	Young's modulus (kPa)
Normal fat	3.25 ± 0.91
Normal fibroglandular tissue	3.24 ± 0.61
Fibroadenoma	6.41 ± 2.86
DCIS (ductal carcinoma in situ)	16.38 ± 1.55
Low-grade IDC (invasive ductal carcinoma)	10.40 ± 2.60
High-grade IDC	42.52 ± 12.47

Table 2a Elastography methods. Each column shows methods and measured parameters for elastography. Each row shows a method for inducing displacement. Each cell shows a type of elastography.

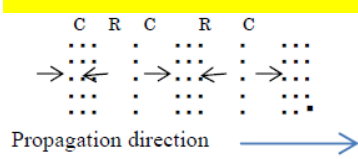
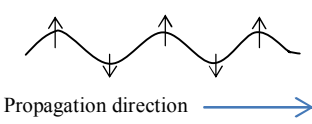
Measured physical quantity Methods Excitation methods	Strain or Displacement 	Shear wave speed 
	Strain imaging	Shear wave imaging
(A) Manual compression -Palpation, -Cardiovascular Pulsation -Respiration	Strain elastography	
	-ElaXto™, Esaote -Real-time tissue elastography™, Hitachi Aloka -Elastography, GE, Philips, Toshiba -ElastoScan™, Samsung -eSieTouch™ Elasticity Imaging, Siemens 	
(B) Acoustic radiation force	Acoustic Radiation Force Impulse (ARFI) Imaging	
	-Virtual Touch™ Imaging (VTI), Siemens 	Point shear wave elastography (average shear wave speed in local region) -Virtual Touch™ Quantification (VTQ), Siemens -ElastPQ™, Philips 
(C) Mechanical impulse	Shear wave elastography (Shear wave speed imaging)	
		-ShearWave™ Elastography :SWE, SSI -Virtual Touch™ Image Quantification (VTIQ), Siemens Transient elastography (Average shear wave speed measurement) -FibroScan™, Echosens 

“Point” measurement denotes the fact that measurements are performed in a small region of interest, typically 1 cm², as compared to the entire field of view in the image.

Table 2b Elastography output measures. Each column shows methods for elastography. Each row shows a method for inducing displacement. Each cell shows one or more output measures.

Elastography methods Excitation methods	Strain imaging	Shear wave imaging
(A) Manual compression -Palpation, -Cardiovascular Pulsation -Respiratory	Strain elastography -Geometric measures -Strain ratio -E/B size ratio	
(B) Acoustic radiation force	Acoustic Radiation Force Impulse (ARFI) Imaging -Geometric measures -E/B size ratio	Point shear wave elastography -Shear wave speed -Young's modulus Shear wave elastography -Shear wave speed -Young's modulus
(C) Mechanical impulse		Transient elastography -Young's modulus

Table A1 Longitudinal waves and transverse waves

	Direction of propagation and vibration	Sound speed	Main use (frequency)
Longitudinal wave (compression wave)		$c_L = \sqrt{\frac{K}{\rho}}$ $K \doteq 2\text{GPa}$ Soft tissue $c_L \doteq 1500 \text{ m/s}$,	Imaging by pulse-echo method (MHz band)
Transverse wave (shear wave)		$c_s = \sqrt{\frac{G}{\rho}}$ $G = 1 \sim 100\text{kPa}$ Soft tissue $c_s = 1 \sim 10 \text{ m/s}$	Elastography ($\leq 1\text{kHz}$)

C: Compression, R: Rarefaction

Table A2 Comparison of speckle tracking method and Doppler method

Method Feature	Spatial correlation method (Speckle tracking method)	Phase difference detection method (Doppler method)
Displacement vector	2D measurement possible	1D displacement (due to angle dependence)
Displacement amount	Displacement exceeding wavelength applicable	Up to about half of wavelength (due to aliasing)
Real-time capability	Enormous computational complexity	High-speed operation easy
Noise tolerance	Low	High

1. External mechanical action
2. Estimation of mechanical characteristics (elasticity, viscosity) based on reaction (strain, shear wave propagation)

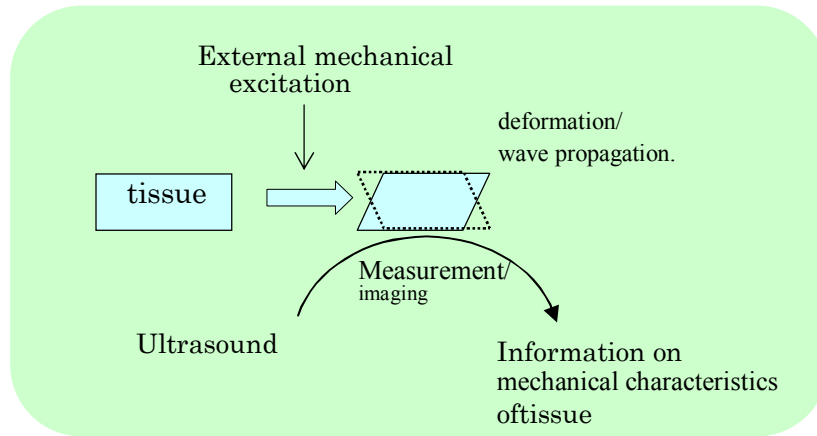


Figure 1 Concept of measurement of tissue elasticity

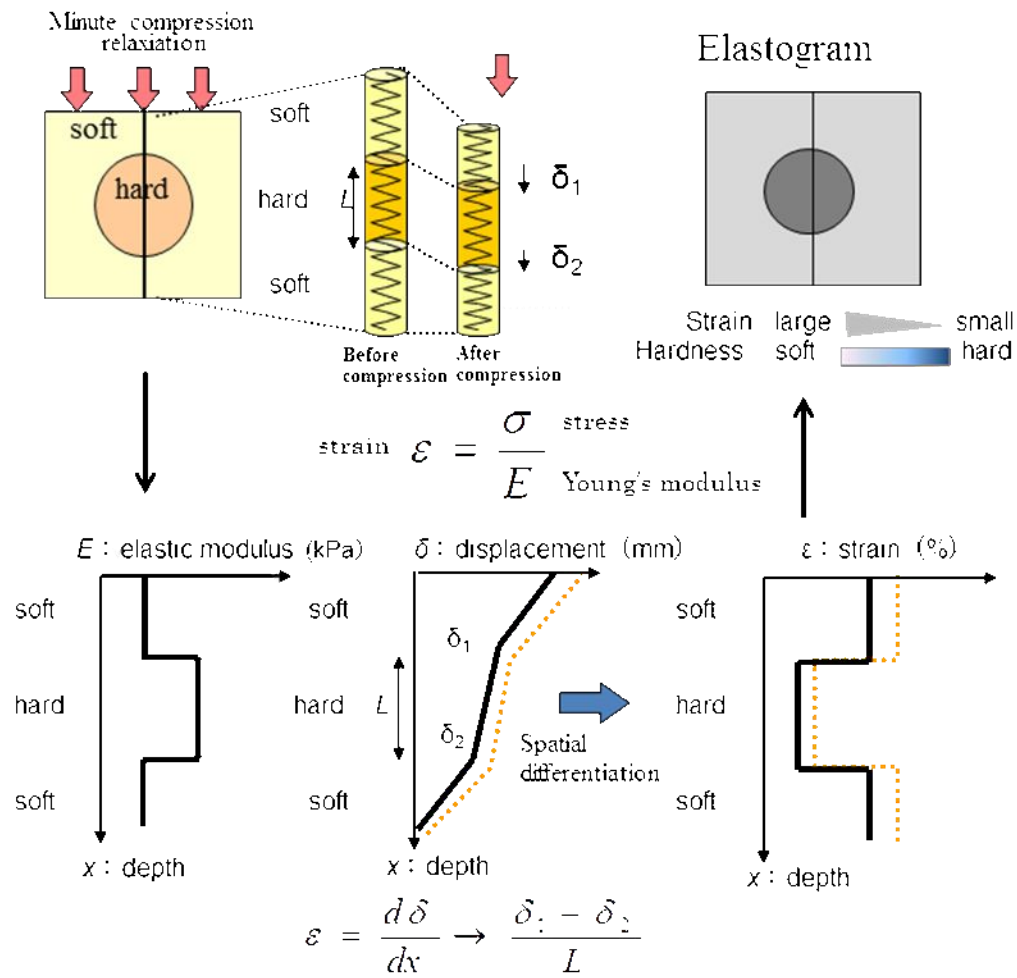
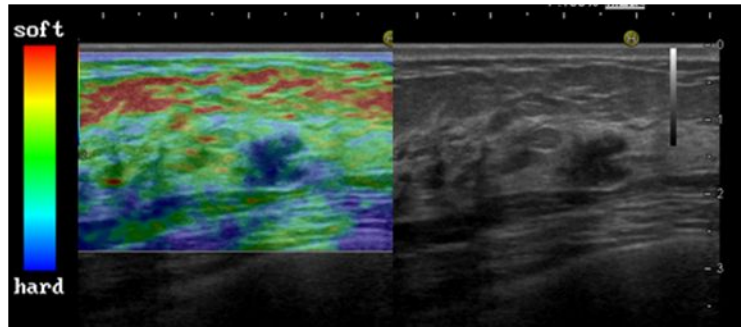


Figure 2 Principle of strain elastography

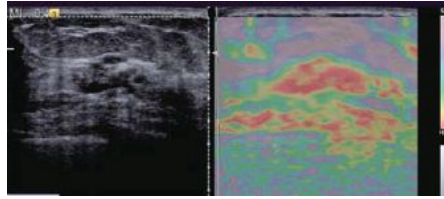
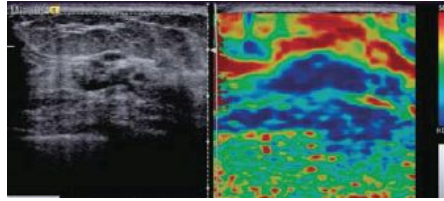


(b) Elastogram (breast cancer)

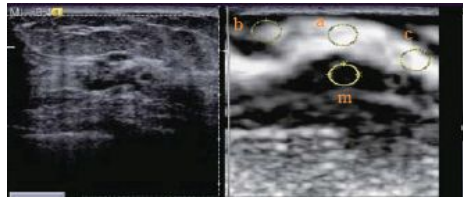
(c) B-mode

(a) First practical ultrasound elastography equipment which was released for breast examination in 2003 (Real-Time Tissue Elastography, Hitachi Aloka Ltd.)

Figure 3 Practical application of strain imaging

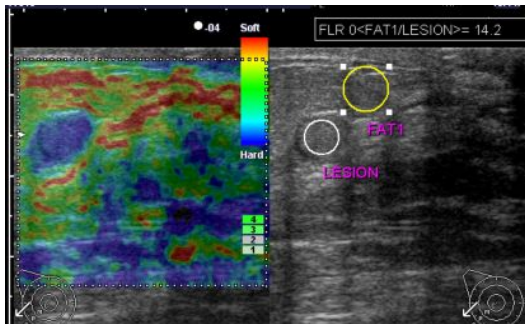


(a)Color elastogram (strain image) superimposed on B-mode image

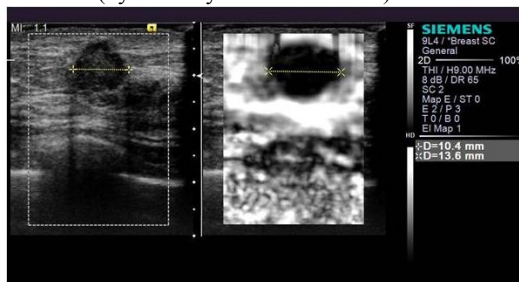


(b)Elastogram with gray scale

Figure 4 Different display methods of strain image.(by courtesy of SIEMENS)



(a) Measurement of strain ratio
(by courtesy of Hitachi Aloka)



(b) Measurement of tumor size based on
elastogram and comparison with B-mode image.
(by courtesy of SIEMENS)

Figure 5 Quantitative diagnosis based on
strain imaging

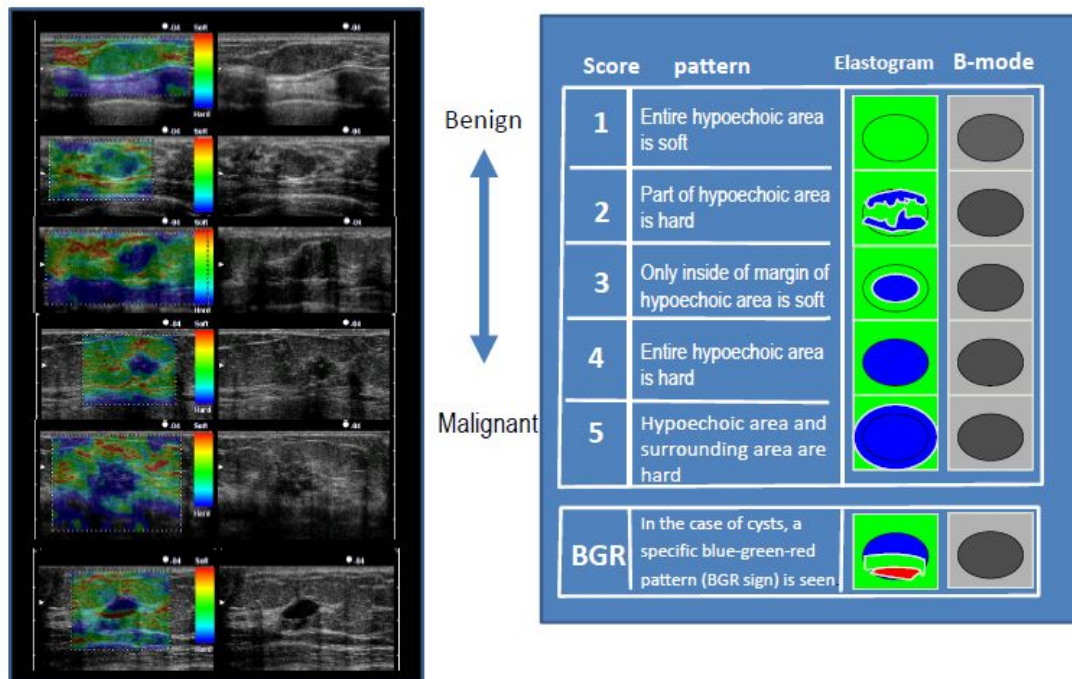


Figure 6 Elasticity score in breast cancer diagnosis

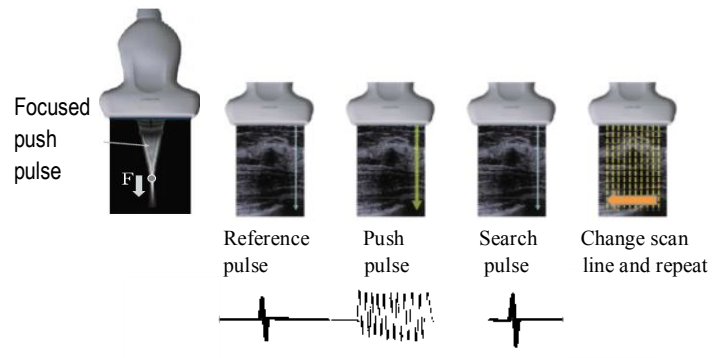
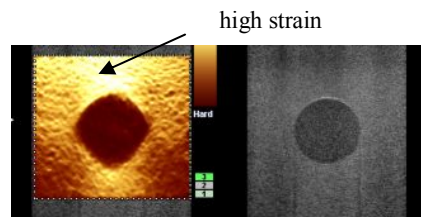


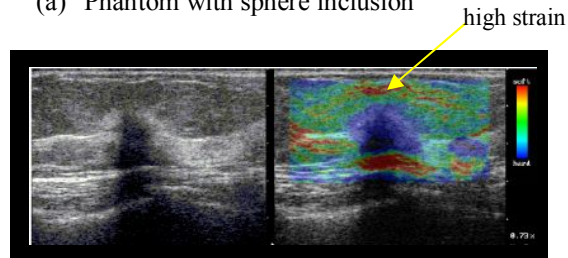
Figure 7 Pulse sequence in ARFI imaging. ARFI imaging utilizes acoustic push pulses and tracking beams, sequenced across a user-defined region of interest, to generate an elastogram depicting the relative stiffness of tissue.



Fig. 8. An image by ARFI imaging



Elastogram B-mode
(a) Phantom with sphere inclusion



(b) Breast cancer (schirus)

Figure 9 Artifacts due to stress concentration

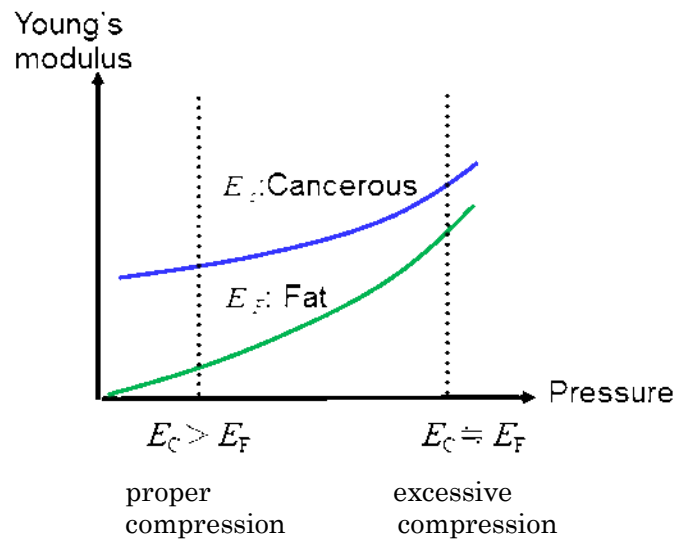
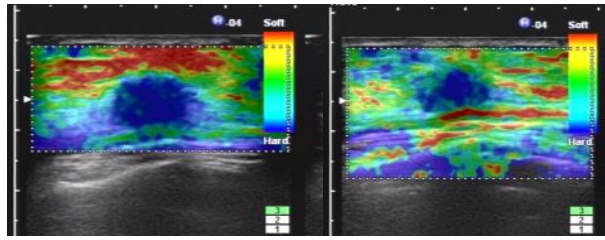
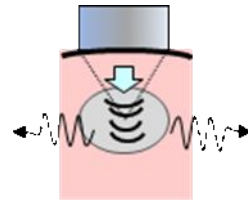
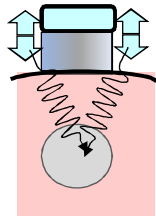


Figure 10 Change in contrast according to nonlinearity of tissue elasticity. When compression is increased, the tissue stiffens and the contrast between fat and a cancerous mass decrease.



(a) Adequate compression (b) Excessive compression

Figure 11 Effect of excessive compression (breast cancer)



(a) Mechanical excitation

(b) Acoustic radiation force based methods

Figure 12 Shear wave generation methods

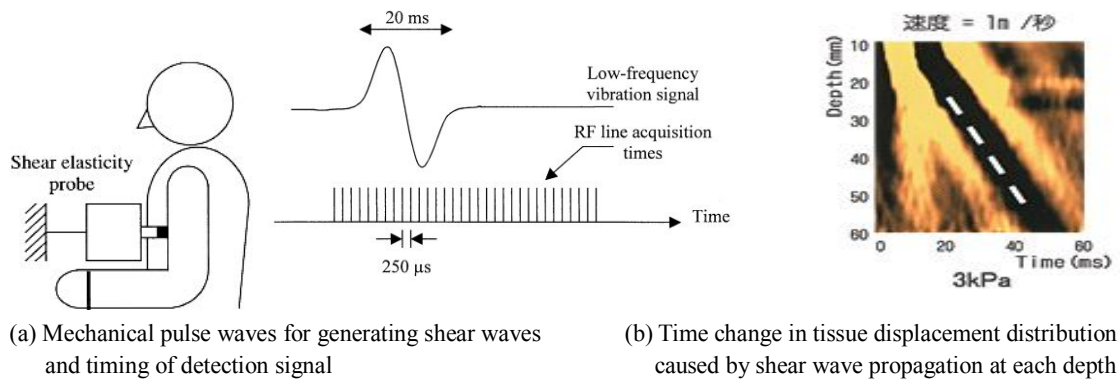
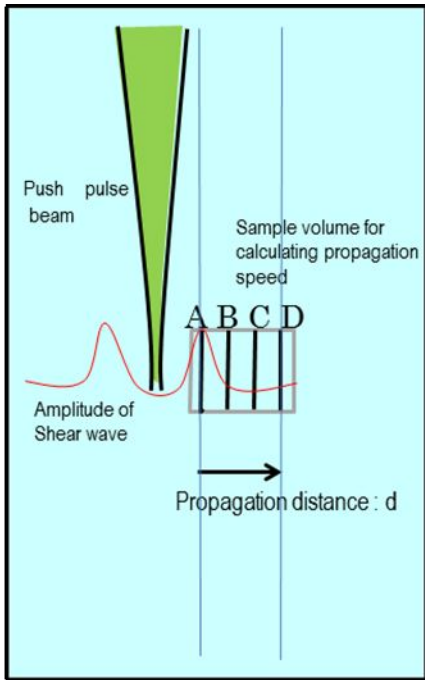
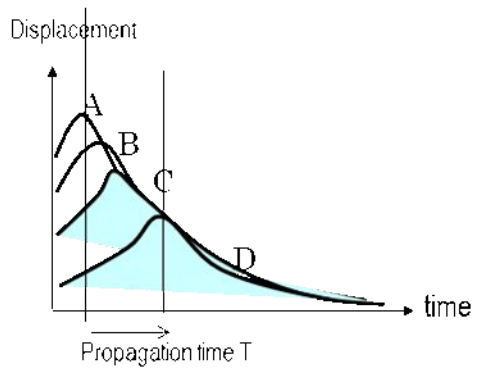


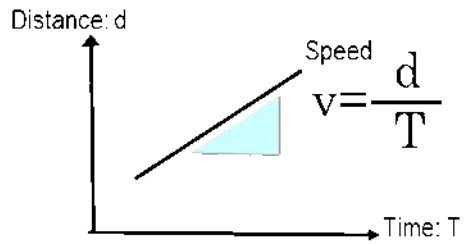
Figure 13 Principle of transient elastography (FibroScan™)



(a) Generation and measurement of shear waves

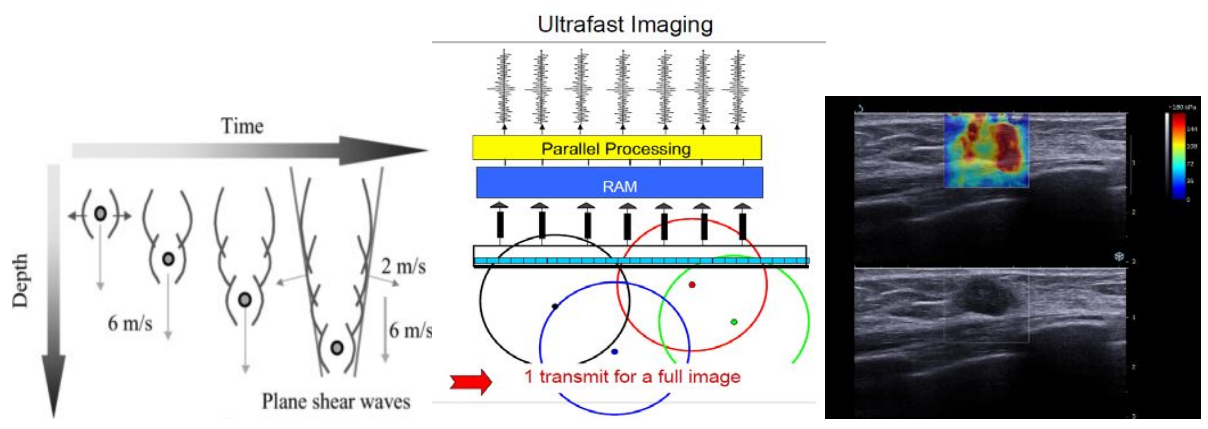


(b) Time profiles of displacement at adjacent positions



(c) Measurement of shear wave speed

Figure 14 Measurement of propagation speed of shear waves



(a) Formation of shear wave wavefront by movement of push pulse focal point

(b) High-speed measurement of displacement by plane wave transmission

(c) An example of shear wave elastography image

Figure 15 Shear wave excitation and high-speed measurement by SWE

Shear waves are generated by multi-focal zone configuration in which each focal zone is interrogated in rapid succession, leading to a cylindrically shaped shear wave extending over a larger depth as shown in (a). Unlike the regular method of focusing during transmission, by simultaneously performing aperture synthesis by transmitting plane waves for the displacement detection method as shown in (b), the incoming data are acquired at high speed, i.e., about 5,000 frames/sec, which is almost 100 fold, and the propagation velocity distribution within the ROI is obtained.

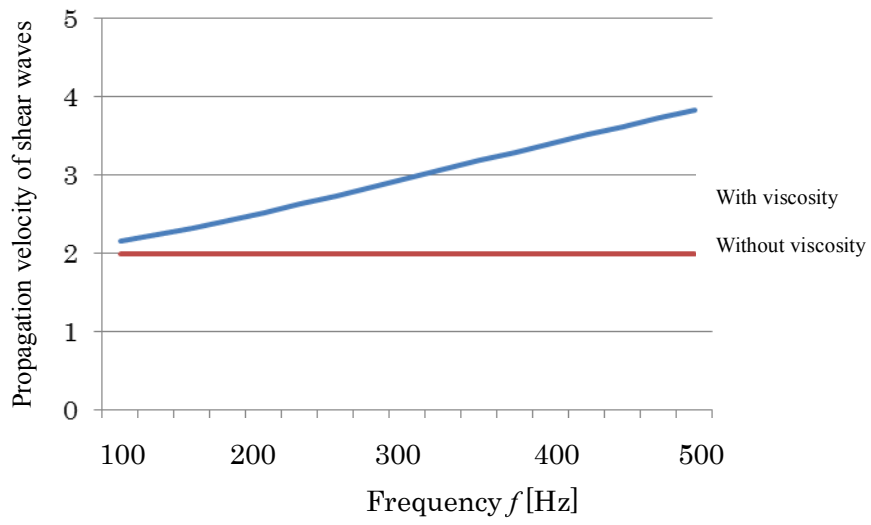
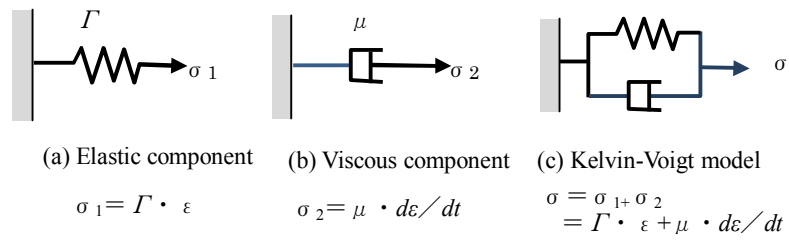


Figure 16 Difference in propagation velocity according to presence or absence of viscosity ($G=4\text{ kPa}$, $\mu=3\text{ Pa}\cdot\text{s}$)



σ : Stress, ε : Strain, Γ : Elastic modulus, μ : Viscosity coefficient

Figure A1 Viscoelastic model

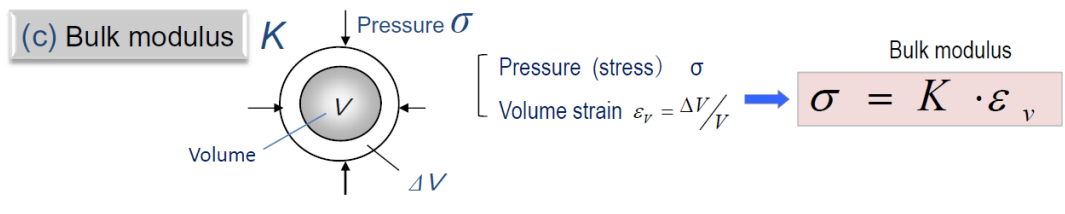
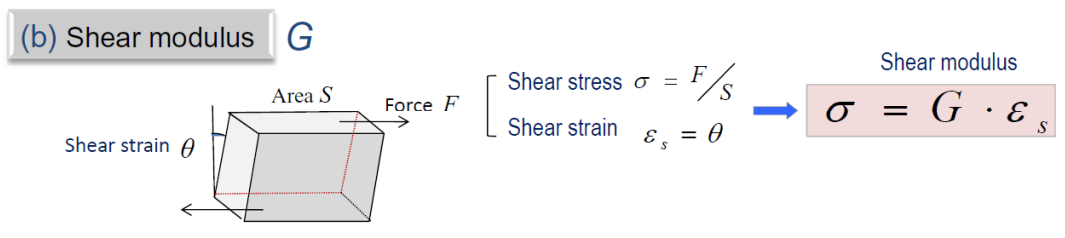
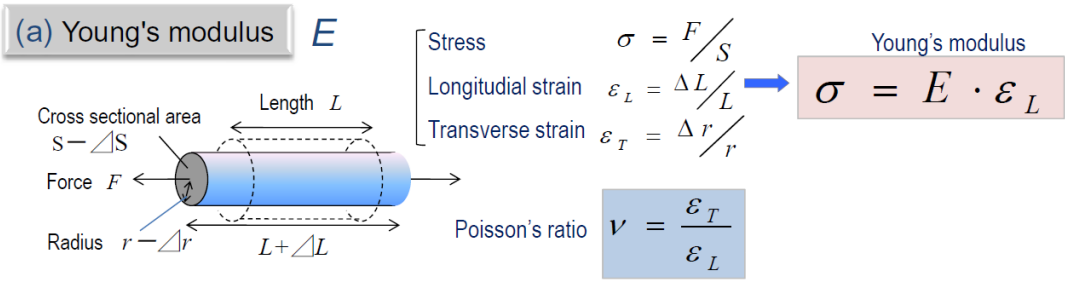
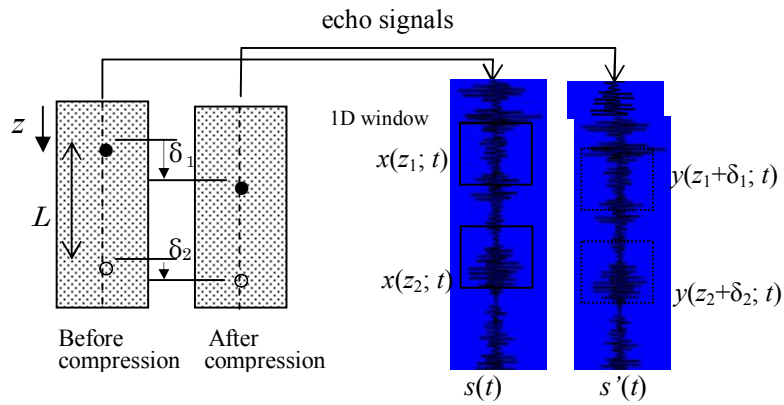
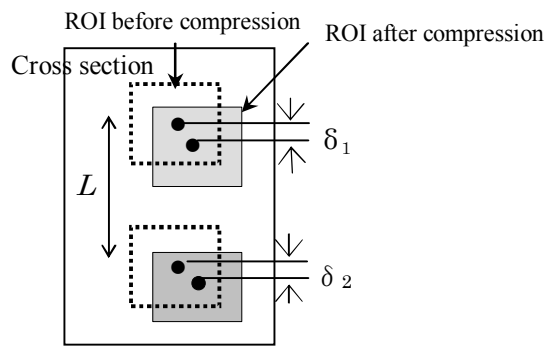


Figure A2 Various elastic moduli



$$R(\delta) = \frac{\int x(z; t)y(z + \delta; t)dt}{\sqrt{\int x^2(z; t)dt \int y^2(z + \delta; t)dt}}$$

(a) Calculation of correlation in 1D window



(b) Calculation of correlation in 2D window

Figure A3 Calculation of correlation using spatial correlation

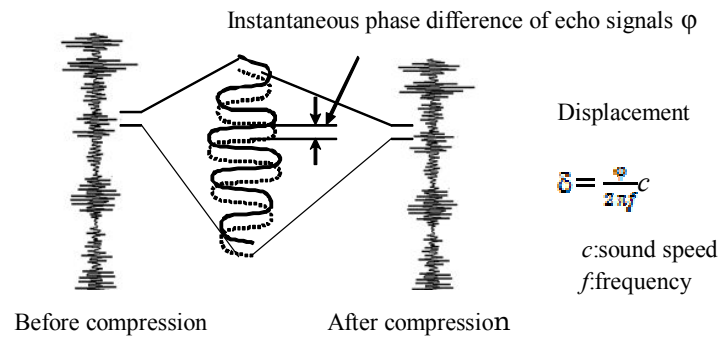


Figure A4 Measurement of displacement by phase difference detection method

Combined Autocorrelation Method (CAM)

● 2 steps

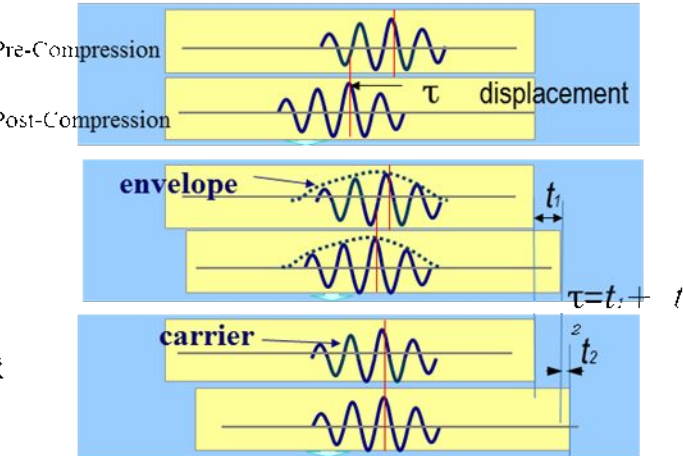
Step1 : Coarse estimation

- Detect large displacement from envelopes
- Select optimal zone without aliasing

Step2 : Fine estimation

- Detect unwrapped phase shift from carriers

Both steps are processed by autocorrelation method



- Improvement in the accuracy
- Large dynamic range of strain (0.05% to 5.0 %)

- Grid correlation → Improvement in the processing speed
→ Optimize computing efficiency without aliasing
- 2-D search → Robust to the slip of probe
→ Freehand compression

CAM is suitable to real time and palpation-like free-hand elasticity evaluation

Figure A5 Principle of the combined autocorrelation method